Dynamics of mobile coupled phase oscillators

Koichiro Uriu,[1,2,3,*] Saúl Ares,[3,4,5] Andrew C. Oates,[2] and Luis G. Morelli[2,3,6,†]

[1]*Theoretical Biology Laboratory, RIKEN Advanced Science Institute, 2-1 Hirosawa, Wako, Saitama 351-0198, Japan*

[2]*Max Planck Institute of Molecular Cell Biology and Genetics, Pfotenhauerstr. 108, 01307 Dresden, Germany*

[3]*Max Planck Institute for the Physics of Complex Systems, Nöthnitzer Str. 38, 01187 Dresden, Germany*

[4]*Logic of Genomic Systems Laboratory, Centro Nacional de Biotecnología, CSIC, Calle Darwin 3, 28049 Madrid, Spain*

[5]*Grupo Interdisciplinar de Sistemas Complejos (GISC)*

[6]*Departamento de Física, FCEyN UBA and IFIBA, CONICET; Pabellón 1, Ciudad Universitaria, 1428 Buenos Aires, Argentina*

(Received 23 July 2012; revised manuscript received 24 January 2013; published 21 March 2013)

We study the transient synchronization dynamics of locally coupled phase oscillators moving on a one-dimensional lattice. Analysis of spatial phase correlation shows that mobility speeds up relaxation of spatial modes and leads to faster synchronization. We show that when mobility becomes sufficiently high, it does not allow spatial modes to form and the population of oscillators behaves like a mean-field system. Estimating the relaxation timescale of the longest spatial mode and comparing it with systems with long-range coupling, we reveal how mobility effectively extends the interaction range.

DOI: 10.1103/PhysRevE.87.032911 PACS number(s): 05.45.Xt, 87.18.Gh, 87.18.Hf

I. INTRODUCTION

The flow of information in systems of mobile agents is relevant to diverse fields of science and technology [1–6]. A fundamental question is how the mobility of agents affects the dynamics of information spreading. The synchronization of locally interacting, mobile oscillators provides an example to address this question. Through the exchange of information, a population of coupled oscillators can self-organize to produce collective rhythms [7–9]. The flow of information across the population depends on the coupling topology, that is, how the oscillators are connected with each other [10,11]. Since interactions often have a finite range [2,12,13], coupling with local neighbors is common in natural systems and in technological applications. In a variety of contexts, locally coupled oscillators can move around and exchange their neighbors [2,13,14]. For example, in robotics, moving robots can generate organized collective motions via local interactions with wireless sensors [2,14]. In somitogenesis in vertebrate embryos, cells with genetic oscillators move around in a tissue and interact with their local neighbors through membrane proteins to synchronize their oscillations [13].

The synchronization of mobile coupled oscillators has been studied using different theoretical approaches [2,14–29]. In technological applications, this problem has been formulated as synchronization on a time varying network [2,15,17,18,21,22,25,26,29]. In some of those studies, the state of oscillators can influence their movement, leading to the self-organization of complex structures among oscillators [15,16,20,21]. In the other studies, the movement of oscillators is independent from their state, allowing the effect of mobility on synchronization to be examined. These latter studies have revealed a significant impact of mobility on synchronization by comparing the dynamics of mobile oscillators with that of nonmobile ones.

The mobility of locally coupled oscillators influences the stability of the steady states of a system. A population of locally coupled nonmobile oscillators tends to form traveling waves, instead of synchronizing across the system in one-dimensional systems with periodic boundary conditions [24] and in two-dimensional systems [23]. The mobility of oscillators promotes the realization of synchronization as a steady state by destabilizing traveling waves in these systems [23,24]. Furthermore, the mobility of oscillators can stabilize the synchronized steady state in the presence of noise [17–19,22,29].

It has been shown that mobility affects transient dynamics, making the approach to synchronization faster [23,25–28]. Despite this progress, it is still unclear how the mobility of oscillators influences the decay of spatial patterns observed in the dynamics toward synchronization. In addition, since mobility allows oscillators to interact with previously distant neighbors, we could expect mobility to effectively extend the interaction range of oscillators, but the relation between mobility and such an effective range remains an open question.

In this paper, we study the transient dynamics of mobile coupled oscillators on a one-dimensional lattice where mobility does not change the steady states but rather affects synchronization dynamics. By measuring a spatial phase correlation, we reveal how the mobility of oscillators accelerates the relaxation of spatial modes. Based on the characteristic relaxation time of the longest spatial mode, we relate mobility to an effective interaction range of oscillators. This effective interaction range increases with the square root of mobility, explaining a mechanism by which mobility enhances synchronization.

II. MOBILE COUPLED PHASE OSCILLATORS

For simplicity, we consider a population of identical oscillators arranged in a one-dimensional lattice of N sites [Fig. 1(a)]. Each oscillator in the lattice is identified by the index j ($j = 0, \ldots, N-1$) and its position is denoted by x_j ($x_j = 0, \ldots, N-1$). We describe oscillator mobility as a Poisson process, by letting them exchange locations with their

*k.uriu@riken.jp

†morelli@df.uba.ar

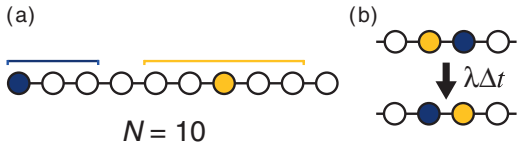

FIG. 1. (Color online) Mobile oscillators on a one-dimensional lattice. (a) Bars indicate a coupling range $r = 2$ for oscillators in the bulk and at a boundary. (b) During a small time interval Δt, each oscillator exchanges its position with one of its adjacent neighbors with probability $\lambda\Delta t$.

nearest neighbors at random times [23,28], and implement it using the Gillespie algorithm [30] [Fig. 1(b)]. Each oscillator performs a random walk on the lattice at a rate λ.

These mobile oscillators can interact with their local neighbors within a coupling range r [Fig. 1(a)]. We use a locally coupled phase oscillator model [31], described in a rotating reference frame:

$$\frac{d\phi_j(t)}{dt} = \frac{\kappa}{n_j} \sum_{|x_{j'}-x_j|\leqslant r} \sin[\phi_{j'}(t) - \phi_j(t)], \qquad (1)$$

where $\phi_j(t)$ is the phase of oscillator j at time t, κ is the coupling strength between oscillators, n_j is the number of oscillators with which oscillator j interacts, and the sum is carried over all oscillators within the coupling range r. Note that each oscillator can interact with oscillators within the range $2r$, but it exchanges its position only with one of its nearest neighbors.

The model includes two independent timescales, one for the phase dynamics represented by $1/\kappa$ and another for the mobility, $1/\lambda$. The ratio λ/κ measures how high mobility is relative to the phase dynamics. In the following, we fix $\kappa = 1$ without loss of generality. The initial phase of each oscillator is chosen randomly from a uniform distribution between 0 and 2π.

We adopt a boundary condition where oscillators in the left and right ends of the lattice interact only with their right and left neighbors, respectively [Fig. 1(a)]. Similarly, an oscillator in an end of the chain can exchange its position only with its single neighboring oscillator. Our numerical simulations show that in finite systems of identical oscillators, phase differences always vanish after a transient regardless of their initial phases and parameters. We refer to the steady state where all phase differences are zero as complete synchronization. The boundary condition we adopt here makes analyzing transient behavior toward synchronization simpler than the periodic boundary condition, which allows spatial patterns to coexist with complete synchronization as stable steady states [24].

III. SPATIAL PHASE CORRELATION

We first consider the case of nearest-neighbor coupling, $r = 1$. Figure 2(a) shows the snapshots of a spatial phase profile for nonmobile oscillators ($\lambda/\kappa = 0$) at different time points. First, the nearest-neighbor coupling for each oscillator balances phase differences between its left and right neighbors. As a result, these nonmobile oscillators tend to form a winding, snaky spatial phase profile comprising several spatial modes with different wavelengths. However, oscillators gradually relax these spatial modes, and in finite systems eventually reach complete synchronization. Thus, there are two timescales for nonmobile oscillators during the achievement of complete synchronization, one for them to form a snaky pattern and the other to relax it. Note that it takes a very long time for these oscillators to relax the snaky pattern and to reach complete synchronization.

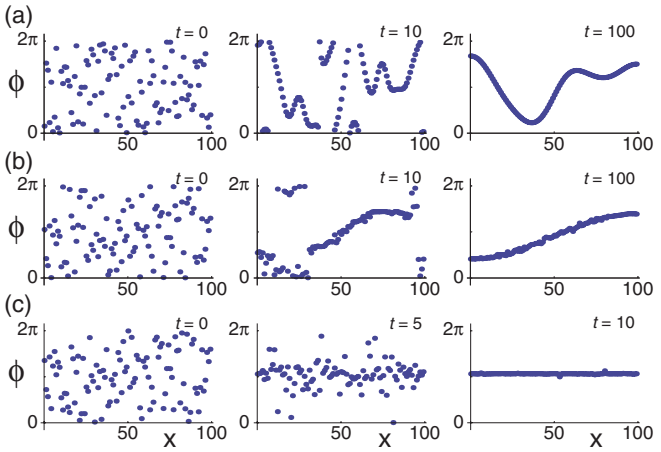

FIG. 2. (Color online) Snapshots of spatial phase profiles. (a) $\lambda/\kappa = 0$, (b) $\lambda/\kappa = 10$, and (c) $\lambda/\kappa = 10^4$. Each dot represents an oscillator. In all panels, $\kappa = 1$, $r = 1$, and $N = 100$.

The transient synchronization dynamics of mobile oscillators is quite different. Figure 2(b) shows the snapshots of a spatial phase profile for oscillators with mobility $\lambda/\kappa = 10$. These oscillators still form a snaky phase pattern from random initial phases, but the pattern is dominated by longer wavelength modes, even at its first appearance. This is because the exchange of neighbors does not allow the nearest-neighbor coupling for each oscillator to balance phase differences with its two neighbors but forces it to synchronize phases of nearby oscillators instead. When mobility is further increased to $\lambda/\kappa = 10^4$, the movement of oscillators precludes the formation of a snaky phase profile by completely breaking local phase order [Fig. 2(c)]. Due to the very short interaction times, each oscillator cannot synchronize its phase with neighbors before moving again. However, all oscillators seem to be attracted to the mean phase of the population, speeding up complete synchronization [Fig. 2(c)].

To characterize the transient dynamics described above, we introduce a correlation between two lattice sites:

$$\rho(d,t) = \langle \cos[\vartheta_{k+d}(t) - \vartheta_k(t)] \rangle_k, \qquad (2)$$

where $\vartheta_k(t)$ is the phase value at site k at time t, d is the distance between two sites ($d = 1, \ldots, N-1$), and $\langle \ldots \rangle_k$ represents the average over different k ($k = 0, \ldots, N-1-d$). If two sites at distance d have similar phases on average, then $\rho \sim 1$. In contrast, if they have opposite phases on average, $\rho \sim -1$. If there is no correlation at this distance, $\rho \approx 0$. We calculate an average of $\rho(d,t)$ over 200 different realizations of initial conditions and movement of oscillators.

Figure 3(a) shows the time evolution of the correlation $\rho(d)$ for nonmobile oscillators. Correlations start increasing sequentially, from shorter to longer ranges. This captures the fact that nonmobile oscillators first form local phase order

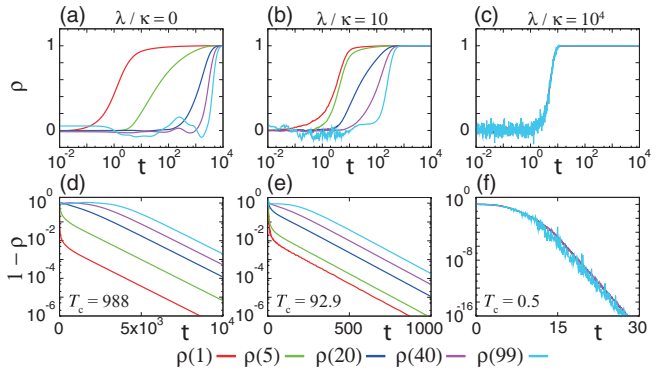

FIG. 3. (Color online) Time evolution of the correlations ρ defined by Eq. (2), (a)–(c), and $1-\rho$, (d)–(f). $\lambda/\kappa = 0$ in (a) and (d), $\lambda/\kappa = 10$ in (b) and (e), $\lambda/\kappa = 10^4$ in (c) and (f). Lines of different colors represent correlations for different distances d, as indicated in the figure. In all panels, $\kappa = 1$, $r = 1$, and $N = 100$; from left to right, the lines are $\rho(1)$, $\rho(5)$, $\rho(20)$, $\rho(40)$, and $\rho(99)$.

structures, which are visible as a snaky spatial phase profile, and then gradually approach global phase order by relaxing spatial modes [Fig. 2(a)]. Relaxation of the snaky pattern is best observed in the behavior of $1-\rho(d)$ [Fig. 3(d)]. After a transient, only the longest spatial mode survives, and correlations show an exponential relaxation described by $1-\rho(d) \propto e^{-t/T_c}$. In this regime we can estimate a characteristic time T_c by fitting this exponential function to the data obtained by numerical simulations. Note that T_c does not depend on d, but for a longer-range correlation the exponential decay occurs much later than for a shorter-range correlation. The phase profile can encompass phase differences larger than 2π [24]. As this difference becomes smaller, the longest-range correlation oscillates. However, the average of the correlation over different initial conditions cancels out this oscillatory behavior, making the start of the exponential decay in $1-\rho(N-1)$ a signature of the phase differences between the most distant sites having become smaller than π.

For mobile oscillators with nearest-neighbor coupling, the growth of the shortest-range correlation $\rho(1)$ is delayed [Fig. 3(b)]. Correlations $\rho(1)$ and $\rho(5)$ start to increase at roughly the same time, indicating that oscillators within this range effectively interact with each other. Growth of the longest-range correlation $\rho(N-1)$ occurs much earlier than for nonmobile oscillators [Figs. 3(b) and 3(e)]. Mobile oscillators also relax the longest spatial mode much faster than nonmobile oscillators, as indicated by a smaller T_c [Fig. 3(e)]. Thus, the mobility of oscillators accelerates the relaxation of snaky phase patterns and the approach to complete synchronization. For even higher mobility, growth of correlations occurs simultaneously for all correlation lengths [Fig. 3(c)]. This indicates the absence of any spatial structure and suggests that the population of oscillators approaches complete synchronization as if each oscillator interacted with all the others. The system exhibits an exponential decay with $T_c \approx 0.5$ [Fig. 3(f)], which coincides with the characteristic time of a mean-field system, $T_{cm} \approx 1/2$ for $\kappa = 1$. High mobility allows each oscillator to meet and interact with all the others in a sufficiently short time and, as a result, these oscillators behave like a mean-field system.

IV. CHARACTERISTIC RELAXATION TIME

To understand how mobility changes the behavior of the system, we examine the dependence of the characteristic time T_c on λ/κ for different system sizes [Fig. 4(a)]. Mobility affects the characteristic time only in an intermediate range: for very low and very high mobility, T_c is independent of λ/κ. For very high mobility, $T_c \approx 0.5$, indicating that the oscillators behave as a mean-field system. For low mobility, T_c depends strongly on system size. By considering the decay of the longest spatial mode in the linearized Eq. (1), we find that $T_c \approx N^2/\pi^2\kappa$ for nonmobile oscillators with nearest-neighbor coupling. Therefore, we can scale the data by introducing $\tilde{T}_c = T_c/(N^2/\pi^2\kappa)$ [Fig. 4(b)]. Within the range between $\lambda/\kappa = 1$ and the onset of mean-field behavior, the characteristic time $\tilde{T}_c$ follows $(\lambda/\kappa)^{-1}$, suggesting that

$$T_c \approx \frac{N^2}{\pi^2\kappa}\frac{1}{1+\lambda/\kappa}. \tag{3}$$

This expression matches precisely the scaled numerical results [Fig. 4(b)].

To derive Eq. (3) analytically, we examine how a single exchange of locations between two oscillators affects the relaxation process of the longest spatial mode. The derivation relies on the assumption that the number of oscillators N is large. We consider a situation in which the coupling range r of each oscillator is small enough such that the longest spatial mode can be approximated by a sinusoidal function [Fig. 5(a)]. We describe the time evolution of the phase at each lattice site in a rotating reference frame:

$$\frac{d\vartheta_k(t)}{dt} = \frac{\kappa}{n_k}\sum_{|k'-k|\leqslant r}\sin[\vartheta_{k'}(t)-\vartheta_k(t)], \tag{4}$$

where ϑ_k is the phase value at site k and n_k is the number of neighboring sites coupled with the site k ($k = 0,1,\ldots,N-1$). Note that we do not describe single oscillators; instead, we consider the time evolution of the phase at each lattice site. We introduce a small perturbation $\varphi_k(t)$ around the completely synchronized state ϑ_0, $\vartheta_k(t) = \vartheta_0 + \varphi_k(t)$, and linearize Eq. (4):

$$\frac{d\varphi_k(t)}{dt} = \frac{\kappa}{n_k}\sum_{|k'-k|\leqslant r}[\varphi_{k'}(t)-\varphi_k(t)]. \tag{5}$$

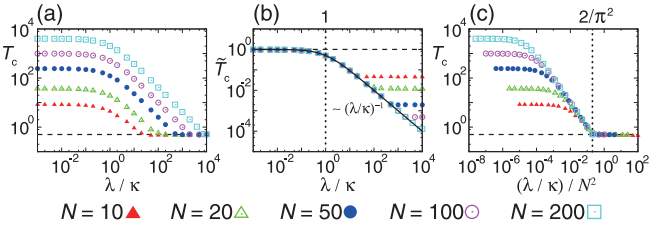

FIG. 4. (Color online) Onset of nonlocal and mean-field behavior. (a) Dependence of the characteristic time T_c on λ/κ for different system sizes. (b) Dependence of the scaled characteristic time $\tilde{T}_c$ on λ/κ. The solid line indicates Eq. (3). The dashed line indicates $\tilde{T}_c = 1$. (c) Dependence of T_c on the scaled moving rate $(\lambda/\kappa)/N^2$. In (a) and (c), the dashed line indicates $T_c = 1/2$. In all panels, $\kappa = 1$ and $r = 1$.

Because Eq. (5) is a system of linear ordinary differential equations, we can write its general solution $\vec{\varphi}(t) = [\varphi_0(t),\varphi_1(t),\ldots,\varphi_{N-1}(t)]^{\mathrm{T}}$ between two successive exchange events as:

$$\vec{\varphi}(t) = \mathrm{e}^{\sigma_0 t}\epsilon_0\vec{v}_0 + \mathrm{e}^{\sigma_1 t}\epsilon_1\vec{v}_1 + \cdots + \mathrm{e}^{\sigma_{N-1}t}\epsilon_{N-1}\vec{v}_{N-1}, \quad (6)$$

where ϵ_i are small constants determined by the initial condition, σ_i is the eigenvalue of the linearized matrix corresponding to Eq. (5), and $\vec{v}_i = [v_{0i}, v_{1i}, \ldots, v_{N-1i}]^{\mathrm{T}}$ is the eigenvector associated to the eigenvalue σ_i ($i = 0,1,\ldots,N-1$). We choose orthonormal eigenvectors, such that their scalar products are $\vec{v}_i \cdot \vec{v}_j = \delta_{ij}$. Since the synchronized state ϑ_0 is always stable, we can sort the eigenvalues as $\sigma_{N-1} < \sigma_{N-2} < \cdots < \sigma_1 < \sigma_0 = 0$. The eigenvector $\vec{v}_0 = \sqrt{1/N}\,[1,1,\ldots,1]^{\mathrm{T}}$ is the spatially uniform mode. The eigenvector $\vec{v}_1$ represents the longest spatial mode with components $v_{k1} \approx \sqrt{2/N}\cos(\pi k/N)$. Its characteristic relaxation time $|\sigma_1|^{-1}$ is the slowest among all nonuniform modes [Fig. 3]. Note that σ_i and $\vec{v}_i$ in Eq. (6) are the same as those in a corresponding system of nonmobile oscillators. Therefore, by substituting $\vec{\varphi}(t) = \mathrm{e}^{\sigma_1 t}\epsilon_1\vec{v}_1$ in Eq. (5), we obtain

$$\sigma_1 \approx -\frac{\pi^2\kappa(r+1)(2r+1)}{12N^2}. \quad (7)$$

Below, we approximate the effect of exchange events by introducing time-dependent coefficients $\epsilon_i(t)$ in Eq. (6). We derive an expression for the time evolution of $\epsilon_1(t)$ to obtain an effective characteristic timescale for the relaxation of the longest spatial mode.

Suppose that by the time t_0 shorter spatial modes have disappeared almost completely, and the solution Eq. (6) can be approximated by the longest spatial mode $\vec{v}_1$ alone [Fig. 5(a)]. Let $\vec{\varphi}_0 \equiv \vec{\varphi}(t_0)$ be this solution at $t = t_0$. We can determine ϵ_i in Eq. (6) by solving

$$\vec{\epsilon}(t_0) = \mathbf{V}(t_0)^{-1}\vec{\varphi}_0, \quad (8)$$

where $\vec{\epsilon}(t_0) = [\epsilon_0(t_0),\epsilon_1(t_0),\ldots,\epsilon_{N-1}(t_0)]^{\mathrm{T}}$ and $\mathbf{V}(t_0) = [\mathrm{e}^{\sigma_0 t_0}\vec{v}_0, \mathrm{e}^{\sigma_1 t_0}\vec{v}_1, \ldots, \mathrm{e}^{\sigma_{N-1}t_0}\vec{v}_{N-1}]$. $|\epsilon_i(t_0)/\epsilon_1(t_0)| \ll 1$ for $i = 2,3,\ldots,N-1$ because $\vec{\varphi}_0$ is well approximated by the longest spatial mode.

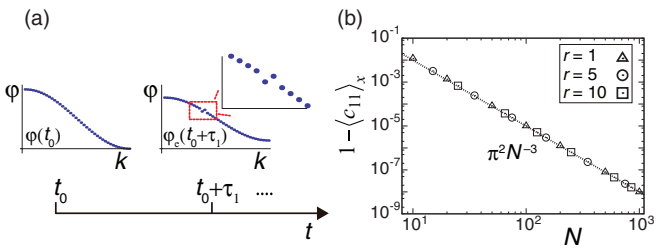

FIG. 5. (Color online) Effect of a single exchange event on the longest spatial mode. (a) Shape of the longest spatial mode and a small defect caused by an exchange event between two neighboring oscillators at time $t = t_0 + \tau_1$. Each dot indicates an oscillator. See text for symbols. (b) Dependence of $1 - \langle c_{11}\rangle_x$ on system size N for different coupling ranges r. Symbols indicate the results obtained from a numerical calculation where we first compute $c_{11}(x)$ for each x and then compute its spatial average $\langle c_{11}\rangle_x$. The broken line is π^2/N^3, as in Eq. (17).

Suppose that at the time $t_1 = t_0 + \tau_1$, the first exchange event after t_0 happens between a pair of oscillators in sites $k = x_1$ and $k+1 = x_1+1$ in the system ($x_1 = 0,1,\ldots,N-2$) [Fig. 5(a)]. Just before the exchange event, the solution of Eq. (5) can be written as

$$\vec{\varphi}(t_1) = \mathrm{e}^{\sigma_0 t_1}\epsilon_0(t_0)\vec{v}_0 + \mathrm{e}^{\sigma_1 t_1}\epsilon_1(t_0)\vec{v}_1 + \cdots + \mathrm{e}^{\sigma_{N-1}t_1}\epsilon_{N-1}(t_0)\vec{v}_{N-1}. \quad (9)$$

The exchange event introduces a defect in the solution described by Eq. (9). The phase values $\vec{\varphi}_{\mathrm{e}}(t_1)$ at each lattice site immediately after the exchange event are obtained by exchanging the x_1 component of $\vec{\varphi}(t_1)$ with its x_1+1 component:

$$\vec{\varphi}_{\mathrm{e}}(t_1) = \mathrm{e}^{\sigma_0 t_1}\epsilon_0(t_0)\vec{u}_0 + \mathrm{e}^{\sigma_1 t_1}\epsilon_1(t_0)\vec{u}_1 + \cdots + \mathrm{e}^{\sigma_{N-1}t_1}\epsilon_{N-1}(t_0)\vec{u}_{N-1}, \quad (10)$$

where $\vec{u}_i = [v_{0i},\ldots,v_{x_1-1i},v_{x_1+1i},v_{x_1i},\ldots,v_{N-1i}]^{\mathrm{T}}$. At the time t_1, the solution jumps from $\vec{\varphi}(t_1)$ given by Eq. (9) to $\vec{\varphi}_{\mathrm{e}}(t_1)$ given by Eq. (10).

We write the vectors $\vec{u}_i$ in Eq. (10) as linear combinations of the orthonormal base $\vec{v}_i$, $\vec{u}_i = \Sigma_{j=0}^{N-1} c_{ji}(x_1)\vec{v}_j$, where $c_{ji}(x_1)$ are coefficients that depend on the location of exchange x_1. Since $\vec{u}_i$ is a small perturbation to $\vec{v}_i$, we argue that $c_{ii}(x_1) \sim O(1)$ and $c_{ji}(x_1) \sim O(\gamma)$, where $i \neq j$ and $\gamma \ll 1$. By substituting this expression into Eq. (10), we obtain

$$\vec{\varphi}_e(t_1) = \mathrm{e}^{\sigma_0 t_1}\epsilon_0(t_1)\vec{v}_0 + \mathrm{e}^{\sigma_1 t_1}\epsilon_1(t_1)\vec{v}_1 + \cdots + \mathrm{e}^{\sigma_{N-1}t_1}\epsilon_{N-1}(t_1)\vec{v}_{N-1}, \quad (11)$$

where we have introduced rescaled coefficients:

$$\epsilon_i(t_1) \equiv \epsilon_i(t_0)\sum_{j=0}^{N-1} c_{ij}(x_1)\mathrm{e}^{(\sigma_j-\sigma_i)t_1}\epsilon_j(t_0)/\epsilon_i(t_0). \quad (12)$$

If we compare Eq. (11) with Eq. (9), we see that we describe the effect of the exchange event as a time-dependent coefficient for each eigenmode.

Next, we will approximate these time-dependent coefficients to find the effective characteristic relaxation time of the longest spatial mode in the presence of exchange events. From Eq. (12), the coefficient for the longest spatial mode is

$$\epsilon_1(t_1) \equiv \epsilon_1(t_0)\left\{c_{11}(x_1) + \frac{\mathrm{e}^{\sigma_2 t_1}\epsilon_2(t_0)}{\mathrm{e}^{\sigma_1 t_1}\epsilon_1(t_0)}c_{12}(x_1) + \cdots + \frac{\mathrm{e}^{\sigma_{N-1}t_1}\epsilon_{N-1}(t_0)}{\mathrm{e}^{\sigma_1 t_1}\epsilon_1(t_0)}c_{1N-1}(x_1)\right\}. \quad (13)$$

If a system is dominated by the longest spatial mode, $|\mathrm{e}^{\sigma_i t_1}\epsilon_i(t_0)/\mathrm{e}^{\sigma_1 t_1}\epsilon_1(t_0)| < 1$ for $i = 2,3,\ldots,N-1$. Because $c_{1i} \sim O(\gamma)$ for $i = 2,3,\ldots,N-1$, we can write Eq. (13) as

$$\epsilon_1(t_1) = \epsilon_1(t_0)\{c_{11}(x_1) + O(\gamma)\}. \quad (14)$$

Since the eigenvectors form an orthonormal base, $c_{11}(x_1) = \vec{v}_1 \cdot \vec{u}_1$.

If exchange events occur subsequently at $t_2 = t_1 + \tau_2$, $t_3 = t_2 + \tau_3, \ldots, t_m = t_{m-1} + \tau_m$ in a system dominated by the longest spatial mode, the time-dependent coefficient of the longest spatial mode will be given by

$$\epsilon_1(t_m) = \epsilon_1(t_0)\left\{\prod_{q=1}^{m} c_{11}(x_q) + O(\gamma)\right\}. \quad (15)$$

Hence, we approximate $\epsilon_1(t_m)$ by the leading order term:

$$\epsilon_1(t_m) \approx \epsilon_1(t_0) \prod_{q=1}^{m} c_{11}(x_q). \tag{16}$$

Assuming that over long timescales exchange events will occur at different locations, sampling evenly $c_{11}(x)$, we approximate the $c_{11}(x_q)$ in Eq. (16) by the spatial average of $c_{11}(x)$:

$$\langle c_{11} \rangle_x = \sum_{x=0}^{N-2} c_{11}(x)/(N-1) \approx 1 - \pi^2/N^3, \tag{17}$$

for $N \gg 1$ [Fig. 5(b)]. The time-dependent coefficient in Eq. (16) can then be approximated by

$$\epsilon_1(t_m) \approx \epsilon_1(t_0)(1 - \pi^2/N^3)^m. \tag{18}$$

Subsequently, we transform the second factor of the right-hand side of Eq. (18) using the relation $(1 - \pi^2/N^3)^m = \exp[m \ln(1 - \pi^2/N^3)]$. Since $\pi^2/N^3 \ll 1$, we expand the logarithm as $\exp[m \ln(1 - \pi^2/N^3)] \approx \exp[-\pi^2 m/N^3]$. Because the average waiting time between two successive exchange events is $\sum_{j=1}^{m} \tau_j/m = (t_m - t_0)/m \approx (\lambda N/2)^{-1}$, the number of exchange events m within the time interval $t_m - t_0$ can be approximated as $m \approx \lambda N(t_m - t_0)/2$. Therefore,

$$\epsilon_1(t) \approx \exp\left[-\frac{\pi^2 \lambda}{2N^2}(t - t_0)\right] \epsilon_1(t_0). \tag{19}$$

Since the system is dominated by the longest spatial mode, we approximate the solution of Eq. (5) under exchange events as

$$\vec{\varphi}(t) \approx e^{\sigma_0 t} \epsilon_0(t) \vec{v}_0 + e^{\sigma_1 t} \epsilon_1(t) \vec{v}_1. \tag{20}$$

In this approximate expression for the relaxation of the longest spatial mode, the effect of mobility is described by the time-dependent coefficient $\epsilon_1(t)$ and results in an effective relaxation time. By substituting Eq. (19) into Eq. (20), we obtain

$$\vec{\varphi}(t) \approx e^{\sigma_0 t} \epsilon_0(t) \vec{v}_0 + e^{(\sigma_1 - \frac{\pi^2 \lambda}{2N^2})t} \eta \epsilon_1(t_0) \vec{v}_1, \tag{21}$$

where $\eta = \exp(\pi^2 \lambda t_0/2N^2)$. The characteristic time T_c of the correlation ρ defined by Eq. (2) can be expressed as

$$T_c = 1/(2|\sigma_1| + \pi^2 \lambda/N^2). \tag{22}$$

The factor of $1/2$ in this expression for T_c comes from the expansion of the cosine in the definition of the correlation; see Eq. (2). By substituting Eq. (7) for $|\sigma_1|$, we obtain

$$T_c = \frac{N^2}{\pi^2 \kappa} \frac{1}{f(r) + \lambda/\kappa}, \tag{23}$$

where

$$f(r) = (r+1)(2r+1)/6. \tag{24}$$

Setting $r = 1$ in Eq. (23) gives Eq. (3). This expression matches precisely the numerical results as long as the ratio λ/κ is smaller than at the onset of mean-field behavior [Fig. 4(b)].

V. ONSET OF NONLOCAL AND MEAN-FIELD BEHAVIOR

Equation (3) indicates that mobility starts to affect the dynamics at $\lambda/\kappa \sim 1$, and this onset of nonlocal behavior does not depend on the system size N [Fig. 4(b)]. This is because in order to disturb the local patterns, oscillators have to move before the coupling restores the balance between neighbors. We can also use this expression to determine the onset of mean-field behavior. Since the characteristic time for a mean-field system is $T_{cm} \approx 1/2\kappa$, Eq. (3) suggests that this onset occurs for

$$\lambda/\kappa \approx 2N^2/\pi^2, \tag{25}$$

as long as $N \gg 1$. By introducing a scaled moving rate $(\lambda/\kappa)/N^2$, the onset of mean-field behavior for different system sizes collapses at around $2/\pi^2$ [Fig. 4(c)], as expected from Eq. (25). Equation (25) shows that mean-field behavior is observed for $(N^2/\lambda)/(1/\kappa) < \pi^2/2$. Since each oscillator performs a random walk in the lattice, the average time for an oscillator to go across the system from one end to the other is N^2/λ. When this timescale becomes similar to that of the phase dynamics $1/\kappa$, each oscillator can meet and interact with all others before their phases change significantly. As a result, on long timescales each oscillator behaves as if coupled to a mean field.

The onset of mean-field behavior seems to occur abruptly at the value of λ/κ predicted by Eq. (25) [Fig. 4(c)], suggesting that there might be a dynamic phase transition. The longest spatial mode is expected to lose stability at this point, and the system approaches complete synchronization without having any characteristic length scales, as in the mean-field regime. Clarifying what kind of transition occurs at the onset of mean-field behavior is an open question that we leave for future work.

VI. EFFECTIVE COUPLING RANGE

As mobility bridges from local to mean-field type behavior, it seems to increase the effective coupling range of the oscillators until it spans the whole system. To introduce a mobility-dependent effective coupling range, we compare the characteristic time T_c in systems of mobile oscillators with that of nonmobile oscillators with a coupling range r. Using Eq. (7) we obtain for nonmobile oscillators:

$$T_c \approx \frac{1}{2|\sigma_1|} \approx \frac{6N^2}{\pi^2 \kappa (r+1)(2r+1)}. \tag{26}$$

Equation (26) gives a good approximation of T_c for nonmobile oscillators when $r/N \ll 1$, and it deviates from numerical results as r increases [Fig. 6(a)]. Equating Eqs. (3) and (26), an effective coupling range of mobile oscillators r_e can be defined as

$$r_e = \frac{-3 + \sqrt{49 + 48\lambda/\kappa}}{4}. \tag{27}$$

Equation (27) is valid in the regime where the longest spatial mode keeps its sinusoidal shape, that is for $(\lambda/\kappa)/N^2 \ll 1$. When $\lambda/\kappa \gg 1$, $r_e^2 \propto \lambda/\kappa$, which can be interpreted as the mean square displacement of an oscillator during the time interval $1/\kappa$ with a diffusion coefficient λ [Fig. 6(b)]. Thus, the mobility of oscillators effectively extends the coupling range.

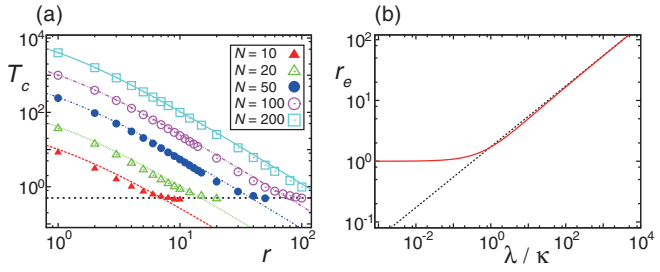

FIG. 6. (Color online) Effective coupling range induced by mobility. (a) Dependence of the characteristic time T_c on the coupling range r for nonmobile oscillators in systems of different sizes N. Symbols correspond to numerical simulations, lines indicate the approximation given by Eq. (26). Parameters: $\kappa = 1$ and $\lambda/\kappa = 0$. (b) Dependence of the effective coupling range r_e given by Eq. (27) on λ/κ. $r = 1$. The dotted line represents $r_e = \sqrt{48}/4 \times \sqrt{\lambda/\kappa}$.

VII. LONG-RANGE COUPLING

In this section, we study the onset of nonlocal and mean-field behavior in a system of mobile oscillators with an arbitrary coupling range r, extending the case $r = 1$ discussed above. Equation (23) provides a good approximation of the characteristic time T_c as compared to its numerical estimation [Fig. 7(a)] and indicates that the effect of mobility becomes apparent when

$$\lambda/\kappa > f(r). \tag{28}$$

If $r \gg 1$ while $r/N \ll 1$, this condition can be approximated as

$$\lambda/\kappa > r^2/3. \tag{29}$$

Equation (29) can be transformed into $(r^2/\lambda)/(1/\kappa) < 3$, indicating that the mobility of oscillators can affect synchronization dynamics when the timescale for each oscillator to explore the coupling range r is comparable to that of the phase dynamics [Fig. 7(a)].

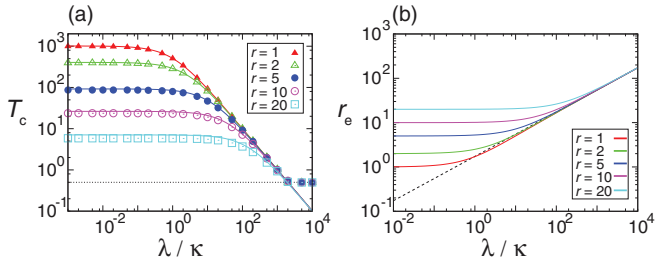

FIG. 7. (Color online) Onset of nonlocal behavior for mobile oscillators with coupling ranges r and their effective coupling range r_e. (a) Dependence of T_c on λ/κ for different coupling ranges r. Symbols indicate T_c obtained by numerical simulations of Eq. (1), while each colored line indicates Eq. (23) for corresponding r of the same color. The horizontal dotted line indicates $T_c = 1/2$. $\kappa = 1$ and $N = 100$. (b) Dependence of the effective coupling range r_e given by Eq. (31) on λ/κ. The dotted line represents $r_e = \sqrt{48}/4 \times \sqrt{\lambda/\kappa}$. From top to bottom, the solid lines are $r = 20, 10, 5, 2, 1$.

The onset of mean-field behavior occurs when $T_c \approx T_{\rm cm} = 1/2\kappa$. Substituting this condition in Eq. (23), we obtain

$$\frac{\lambda}{\kappa} = \frac{2N^2}{\pi^2} - f(r). \tag{30}$$

As long as coupling range is small, $r/N \ll 1$, we can neglect $f(r)$ in Eq. (30). Thus, in contrast to the onset of nonlocal behavior, the onset of mean-field behavior through mobility does not depend on the coupling range r; see also Fig. 7(a). For large r/N, our estimate of T_c is no longer accurate.

Finally, an effective coupling range for mobile oscillators with coupling range r can be defined from Eqs. (23) and (26) as

$$r_e = \frac{-3 + \sqrt{1 + 8(r+1)(2r+1) + 48\lambda/\kappa}}{4}. \tag{31}$$

For small λ/κ, the oscillators stay within the coupling range r in the timescale of phase dynamics $1/\kappa$. In this regime, mobility has no impact and the effective coupling range r_e stays constant or very close to the actual coupling range r [Fig. 7(b)]. In the asymptotic regime of large mobility $\lambda/\kappa \gg r^2$, the effective coupling range scales as $r_e \propto \sqrt{\lambda/\kappa}$ [Fig. 7(b)]. A crossover occurs at an intermediate mobility and can be estimated as the point where the lines defined by these two regimes cross. Thus, the value of mobility that marks the onset of nonlocal behavior scales as $\lambda/\kappa \sim r^2$. Beyond this value of mobility, the random walk takes the oscillators further than their actual coupling range in the timescale relevant to phase dynamics, effectively resulting in an extension of the coupling range.

VIII. DISCUSSION

In this work we have considered mobile coupled oscillators as an example to understand how the mobility of agents affects their collective dynamics. We have presented a framework to relate mobility to an effective interaction range by comparing the dynamics of mobile agents with that of nonmobile agents with a longer interaction range. Because some of our key results are derived in a linear regime, Eqs. (23) and (31), we expect that they will also apply to systems where the linearized equations are the same as those of phase oscillators, such as in models for consensus formation [2]. We have modeled the movement of oscillators as a random walk on the lattice and found that its characteristics appear in the onset of mean-field behavior, Eq. (25), and the expression of the effective coupling range, Eq. (27). Corresponding results for different types of movement will reveal how an effective interaction range of oscillators can be connected to movement in general. Testing the generality of the approach we described in this paper would be an interesting subject for future work.

Here we considered identical oscillators on a one-dimensional lattice for simplicity. In systems of nonidentical oscillators there is a critical coupling strength for synchronization. One may ask whether and how mobility changes its value and the character of the synchronization transition in such systems. In two dimensions, patterns with stable defects, such as vortices, coexist as a steady state with the synchronized solution [32,33]. It will be interesting to study the effect of mobility on the stability of these patterns.

These theoretical findings could be tested, for example, using coupled chemical oscillators, which have been recently realized with chemically loaded microscopic beads [34,35]. While patterns have been observed when the beads are nonmobile and fixed on a plate [34], stirred beads have been shown to synchronize in three dimensions [35]. Since stirring rate in theses experiments controls the mobility of chemical oscillators, this system could be used to study how mobility affects synchronization dynamics.

Physical, chemical, biological, and social systems include mobility of agents to a greater or lesser extent. Our current study shows that mobility of agents changes qualitatively the dynamics of information spreading across spatially distributed systems, by effectively extending the range of local interactions. Therefore, addressing the effects of mobility is key to understanding collective dynamics in distributed systems.

ACKNOWLEDGMENTS

We thank Adrian Jacobo, David Jörg, David Richmond, and Federico Vazquez for helpful comments on the manuscript. K.U. is supported by the Japan Society for the Promotion of Science for Young Scientists. S.A. acknowledges funding from CSIC through the Junta para la Ampliación de Estudios program (JAEDOC014, 2010 call), cofunded by the European Social Fund. A.C.O. and L.G.M. were supported by the Max Planck Society and the European Research Council under the European Communities Seventh Framework Programme (FP7/2007-2013), ERC Grant No. 207634.

[1] S. Eubank, H. Guclu, V. S. A. Kumar, M. V. Marathe, A. Srinivasan, Z. Toroczkai, and N. Wang, Nature (London) **429**, 180 (2004).
[2] W. Ren, R. W. Beard, and E. M. Atkins, IEEE Control. Syst. Mag. **27**, 71 (2007).
[3] P. Friedl and D. Gilmour, Nature Rev. Mol. Cell Biol. **10**, 445 (2009).
[4] C. Song, Z. Qu, N. Blumm, and A. L. Barabasi, Science **327**, 1018 (2010).
[5] B. Kerr, M. A. Riley, M. W. Feldman, and B. J. M. Bohannan, Nature (London) **418**, 171 (2002).
[6] T. Reichenbach, M. Mobilia, and E. Frey, Nature (London) **448**, 1046 (2007).
[7] A. T. Winfree, J. Theor. Biol. **16**, 15 (1967).
[8] Y. Kuramoto, *Chemical Oscillations, Waves, and Turbulence* (Springer, Berlin, 1984).
[9] A. Pikovsky, M. Rosenblum, and J. Kurths, *Synchronization: A Universal Concept in Nonlinear Sciences* (Cambridge University Press, Cambridge, 2008).
[10] J. A. Acebrón, L. L. Bonilla, C. J. Pérez-Vicente, F. Ritort, and R. Spigler, Rev. Mod. Phys. **77**, 137 (2005).
[11] A. Arenas, A. Díaz-Guilera, J. Kurths, Y. Moreno, and C. Zhou, Phys. Rep. **469**, 93 (2008).
[12] J. Buhl, D. J. T. Sumpter, I. D.Couzin, J. J. Hale, E. Despland, E. R. Miller, and S. J. Simpson, Science **312**, 1402 (2006).
[13] O. Pourquié, Cell **145**, 650 (2011).
[14] A. Buscarino, L. Fortuna, M. Frasca, and A. Rizzo, Chaos **16**, 015116 (2006).
[15] J. Ito and K. Kaneko, Phys. Rev. Lett. **88**, 028701 (2001).
[16] T. Shibata and K. Kaneko, Physica D **181**, 197 (2003).
[17] I. V. Belykh, V. N. Belykh, and M. Hasler, Physica D **195**, 188 (2004).
[18] J. D. Skufca and E. M. Bollt, Math. Biosci. Eng. **1**, 347 (2004).
[19] M. Porfiri, D. J. Stilwell, E. M. Bollt, and J. D. Skufca, Physica D **224**, 102 (2006).
[20] D. Tanaka, Phys. Rev. Lett. **99**, 134103 (2007).
[21] T. Gross and B. Blasius, J. R. Soc. Interface **5**, 259 (2008).
[22] M. Frasca, A. Buscarino, A. Rizzo, L. Fortuna, and S. Boccaletti, Phys. Rev. Lett. **100**, 044102 (2008).
[23] K. Uriu, Y. Morishita, and Y. Iwasa, Proc. Natl. Acad. Sci. USA **107**, 4979 (2010).
[24] F. Peruani, E. M. Nicola, and L. G. Morelli, New J. Phys. **12**, 093029 (2010).
[25] N. Fujiwara, J. Kurths, and A. Díaz-Guilera, Phys. Rev. E **83**, 025101 (2011).
[26] N. Fujiwara, J. Kurths, and A. Díaz-Guilera, AIP Conf. Proc. **1389**, 1015 (2011).
[27] L. Prignano, O. Sagarra, P. M. Gleiser, and A. Díaz-Guilera, Int. J. Bifurcat. Chaos **22**, 1250179 (2012).
[28] K. Uriu, S. Ares, A. C. Oates, and L. G. Morelli, Phys. Biol. **9**, 036006 (2012).
[29] M. Frasca, A. Buscarino, A. Rizzo, and L. Fortuna, Phys. Rev. Lett. **108**, 204102 (2012).
[30] D. T. Gillespie, J. Phys. Chem. **81**, 2340 (1977).
[31] H. Sakaguchi, S. Shinomoto, and Y. Kuramoto, Prog. Theor. Phys. **77**, 1005 (1987).
[32] J. M. Kosterlitz and D. J. Thouless, J. Phys. C **6**, 1181 (1973).
[33] M. Cross and P. C. Hohenberg, Rev. Mod. Phys. **65**, 851 (1993).
[34] M. R. Tinsley, A. F. Taylor, Z. Huang, and K. Showalter, Phys. Rev. Lett. **102**, 158301 (2009).
[35] A. F. Taylor, M. R. Tinsley, F. Wang, Z. Y. Huang, and K. Showalter, Science **323**, 614 (2009).